Received: 8 June 2023 | Accepted: 2 April 2024

DOI: 10.1002/maco.202313948

ARTICLE

Materials and Corrosion

Stress corrosion tests for prestressing steels—Part 1: The influence of surface condition and test solution composition on hydrogen charging

Lando Seifert | **Andreas Grunewald** | **Thoralf Müller** | **Gino Ebell**

Bundesanstalt für Materialforschung und -prüfung (BAM), 7.6 Corrosion and Corrosion Protection, Berlin, Germany

Correspondence
Lando Seifert, Bundesanstalt für Materialforschung und -prüfung (BAM), 7.6 Corrosion and Corrosion Protection, Unter den Eichen 87, 12205 Berlin, Germany.
Email: Lando.Seifert@bam.de

Funding information
German Federal Ministry for Economic Affairs and Climate Action (BMWK), Grant/Award Number: 03TNH019/A

Abstract

Tests for assessing prestressing steels' susceptibility to hydrogen-induced stress corrosion cracking are essential for approvals, in-house monitoring, and third-party material testing. According to ISO 15630-3, the time to brittle fracture by constant load under corrosive conditions in thiocyanate test solutions (A or B) at 50°C is measured. In the literature, a high scattering in stress corrosion tests is reported, which questions the integrity of the test procedure. This paper shows the results of studies about the influence of solution composition on hydrogen charging in electrochemical and permeation measurements. Electrochemical experiments show that polished steel surfaces without common drawing layers have more consistent free corrosion currents, polarization resistances, and B-values in solution A with low scattering compared to the solution B experiments. The influence of temperature at 50°C and an ambient temperature of 22°C was also tested.

KEYWORDS

drawing layers, hydrogen-induced stress corrosion cracking, permeation measurements, prestressing steels, stress corrosion tests, surface conditions, test solutions

1 | INTRODUCTION

Due to hydrogen-induced stress corrosion cracking (HISCC), brittle fractures of prestressing steels can damage prestressed concrete structures. Cases of damage due to HISCC are connected to unsuitable construction materials and planning or execution errors.[1,2] Concerning the pre-stressing steels, only robust products with low susceptibility to HISCC should get approval. The testing standard ISO 15630-3 provides methods to test the susceptibility in approvals, continuous surveillance, or material tests by third parties.[3] The so-called stress corrosion test should be able to differentiate between exceptionally high susceptible and low susceptible/robust steels. In the stress corrosion test, prestressing steels are pre-stressed to a specific stress level and brought into contact with a thiocyanate test solution. ISO 15630-3 provides two test solutions for the user. Test solution A consists of distilled or demineralized water and ammonium thiocyanate (NH_4SCN) with a mass fraction of 20%. Test solution B contains distilled or demineralized water, potassium sulfate (K_2SO_4), potassium thiocyanate (KSCN), and potassium chloride (KCl) with concentrations of 5.0 g L^{-1} SO_4^{2-}, 1.0 g L^{-1} SCN^- and 0.5 g L^{-1} Cl^-. During the experiment, the pre-stress level and temperature were kept constant. The time to fracture of the sample must be documented using solution A. In solution B, the criterion for passing the test is an agreed-upon time (2000 h) without fracture. Information on

product-specific minimum and median times in solution A are specified in prEN 10138, parts 1–4.[4]

However, test results with high scattering and minor reproducibility are becoming a problem for the integrity of the test. Examples given:

- The test results using solution B are reported with a high scattering, making it impossible to differentiate the susceptibility of different quenched and tempered prestressing steels to HISCC.[5,6]
- In a round-robin test in solution A, the results of inspection bodies were significantly different, which calls into question the reliability of the HISCC-test method.[7]

Since the early days of prestressed concrete construction, various approaches have been taken to develop suitable test methods and electrolyte solutions.[8] Despite test solutions A and B being given in the same testing standard, ISO 15630-3, test solutions pursue completely other approaches:

- Solution A was composed to simulate harsher corrosive conditions for a quick material-based test. Solution A contains construction-related unrealistically high concentrations of thiocyanate (worse than worst-case), which charges more hydrogen at the same time to the steel than solution B. Solution A pursues to test prestressing steels in the manner of classifying the material-specific susceptibility to HISCC, thus to get a ranking of different prestressing steels.
- Solution B's condition corresponds to those of stressed prestressing steel in the duct before grouting. The composition is adapted to the found duct waters on the prestressed concrete construction sites. The extended testing time of 2000 h is also adapted to practical conditions, as this corresponds to the maximum permitted time in the stressed condition in the duct before grouting. Initially, solution B pursues to observe the practical worst-case behavior of the prestressing steels on the construction site to create a "usage permitted?" test, with the results of Yes or No possible.

Solution A has emerged as the most suitable test solution because of its short testing time, mainly used in quality control and continuous surveillance in Germany. Solution B, on the other hand, is prescribed in Germany for testing new prestressing steel grades. The extended testing time might be accepted as a "safer choice" reaction to the above-described high scattering, especially in test solution A. However, for the approval of new prestressing steels for use in Germany, solution B's condition is losing urgent relevance today since the execution standard DIN 1045-3 for prestressed concrete structures demands prevent the ducts from the ingress of water, which impedes the corrosive environments solution B simulates.[9] Both test solutions, however, cover the full failure mechanism - corrosion initiation as a result of surface conditions, hydrogen uptake, and the effect of absorbed hydrogen on fracture.

This paper searches for alternative corrosive testing conditions to tackle the problem of high scattering, which also meet the following testing aims by common principles of a material testing standard:

- Creation of comparability of corrosive conditions for a comparable hydrogen charging.
- Testing should focus on the susceptibility to HISCC as a material property.
- The creation of practical behavior is not aspired.
- Leveled and low scattering test parameters have aspired to create a ranking test in which the only variable should be the product- or batch-related material property of the prestressing steel's particular alloy/microstructure, geometry, or strength class.

A former publication named the importance of solution composition and temperature parameters as well as the material property on the test result.[10] Surface examinations have shown that the production-related drawing layer, scale layer, or mill scale residues cover the delivery surface unevenly and incompletely, resulting in inhomogeneities and micro crevices. In production, it is tolerated that the prestressing steel is randomly and unevenly covered with the layers. Because layer characteristics like composition or layer adhesion are not documented in production control, the layers are not part of the product specification. Thus, removing the layers without affecting the product's geometry and edge microstructure shall be valid to improve the comparability of corrosive conditions for hydrogen charging. This paper observes the influence of surface conditions, solution composition, and solution temperature on corrosion and hydrogen charging to extend the electrochemical knowledge of this corrosion system and give alternative testing conditions to tackle the problem of high scattering.

- In Section 3.1, advantageous surface conditions for drawing layer removal are investigated.
- The influence of the composition (A or B) and temperature (50°C or 22°C) is studied in electrochemical measurements in Sections 3.2 and 3.3. On the one hand, 50°C was chosen for the temperature, which is the current normative test temperature. On the other hand, a test temperature of 22°C was selected as an alternative to minimize the subsequent testing effort (heating step).

- Possible differences in permeation current densities and hydrogen activity for solutions A and B may also be determined on thin steel membranes in permeation measurements in Section 3.4.

What are the specific corrosion characteristics of solution A compared to solution B with regard to the scattering of corrosion quantities? In search of consistent testing conditions, parameters that provide a uniform course of the corrosion current density i_{corr} with the lowest possible scattering, can be an advantageous choice. Results might explain how common solution A or B test methods are suitable for factory production control or initial type testing. Would it be better to control hydrogen charging during the test?

2 | EXPERIMENTAL

2.1 | Prestressing steel used

Smooth cold-drawn St 1470/1670 prestressing steel wire samples (CDS-1670) with a diameter of 7 mm were provided. The chemical composition of the samples determined by optical emission spectroscopy is shown in Table 1. The chemical composition of the samples corresponds to the specifications in the approval documents of the CDS-1670.

2.2 | Surface modification

Surfaces without drawing layers have been produced by SiC (P80) grinding, turning, or polishing. The radius was reduced by 250 µm for turning to remove the drawing layer. In SiC grinding, specimens have been machined with P80 grit on the grinder to metallic luster, reducing the diameter by 10 µm. The surface was polished to a metallic shine grade with a solid polishing paste on the grinding machine's soft polishing cloth wheel. Additionally, a specific small-area scratch in the drawing layer was intended to recreate damage caused by transport. A marking tool was used to apply a scratch approximately 100 µm deep and 2000 µm wide along the circumference of the wire. Regardless of the surface treatment, all surfaces were cleaned with acetone and a dry soft cloth.

2.3 | Roughness measurement

A tactile roughness measurement was performed according to VDI/VDE 2602 Part 2 using a *Jenoptic Hommel Etamic WD10* instrument on the machined surface modifications. The profile method generated an envelope profile from which the average roughness value R_a and the roughness depth R_z in the longitudinal surface direction were determined and listed in Table 2. The conical diamond stylus tip has a 2 µm radius with an included angle of 90°, and the measuring distance was 4.8 mm each.

2.4 | Determining electrochemical process parameters

The free corrosion potential E_{corr} of a defined steel surface versus Ag|AgCl|KCl(sat.) reference electrode has been measured with a *Gamry Interface 1000E* potentiostat. For this purpose, the samples were immersed in 500 mL of stagnant solution, which was tempered to either 22°C ± 1 or 50°C ± 1K via the double-walled measuring cell using a *Julabo F25-HE* thermostat with a *PT100* temperature sensor. After measuring the free corrosion potential in solutions A and B, the linear polarization resistance method determined the polarization resistance R_P. For this purpose, a three-electrode arrangement consisting of the steel surface as a working electrode, Ag|AgCl|KCl(sat.) electrode as a reference electrode, and a grid of titanium mixed metal oxide as the counter electrode was used. A *Gamry Interface 1000E* potentiostat was also used for this purpose. The differential quotient was determined from the linear change in electrode potential from −5 to +5 mV versus E_{corr} and the corresponding change in current; the potential shift velocity was 1 mV s^{-1}. An IR-drop correction was performed. The R_{IR} was determined using a galvanostatic pulse method (GPM), calculated by the potential drop developed during a 0.3 s pulse of 10 mA cm^{-2} divided by the current value (IR-drop). The sampling rate of the

TABLE 1 Chemical composition of prestressing steel wire used and steel membrane for permeation measurements in mass percentages [mass%].

Steel	C	Si	Mn	P	S	Cr	Ni	Mo	V	Cu	Al	Ti	Nb
CDS-1670	0.833	0.285	0.749	0.010	0.012	0.158	0.059	0.013	0.002	0.090	0.002	<0.001	<0.001
Membrane	0.046	0.013	0.204	0.011	0.012	0.012	0.004	0.001	<0.001	0.009	0.053	<0.001	<0.001

TABLE 2 Surface roughnesses of CDS-1670 in different surface conditions.

Surface condition	R_a [µm]	R_z [µm]
Delivery surface (drawing layer)	(0.33 ± 0.05)	(3.14 ± 0.34)
SiC (P80) ground	(0.61 ± 0.06)	(4.96 ± 0.31)
Turned off	(2.80 ± 0.16)	(13.70 ± 0.72)
Polished	(0.13 ± 0.03)	(1.71 ± 0.48)
Drawing layer scratched	Not applicable (aperiodic)	

Note: Where applicable, average roughness value R_a and roughness depth R_z are given.

potential during GPM was 5 kHz. To assess the corrosion behavior of delivery surfaces and surfaces without drawing layers in solutions A and B at 22°C ± 1 and 50°C ± 1K over a reasonable test period of 70 h, R_P was measured at intervals of 0.5, 1.0, 4.0, 7.0, 10.0, 40.0, and 70.0 h of free corrosion. For the determination of I_{corr} and the Tafel slopes of the anodic and cathodic partial curves (β_a, β_c) of electrochemical current density/potential curve (polarization curve), potentiodynamic measurements from −100 to +100 mV versus open circuit potential with a potential shift velocity of 0.5 mV s^{-1} were performed. Polarization curves were recorded with a delay of 5 s at the same intervals where R_P was measured. Finally, with a 15 min delay in measuring R_P at every interval, GPM was performed to determine the IR-drop, as described above. Test solutions' dissolved oxygen (DO) concentration was measured with a *Hanna Instruments HI 5421* bench meter with a *HI76483* DO probe with a built-in temperature sensor at a normal pressure of 100.3 kPa.

2.5 | Permeation measurement

The permeation measurement was carried out with steel membranes made of unalloyed steel type 1.0978 and a thickness of d of 0.05 mm. The chemical composition is shown in Table 1. The steel membrane separates the charging cell from the oxidation cell; both cells have the same surface area A_{geo} in contact with the solution; it is 1.13 cm^2 each. The ratio of the electrolyte volume to A_{geo} on both sides of the membrane is 194.5 mL cm^{-2}. In the oxidation cell, a three-electrode arrangement was used, with the steel membrane as the working electrode, a silver-silver chloride reference electrode (Ag|AgCl|KCl(sat.)), and a grid of titanium mixed metal oxide as the counter electrode. The surface area of the counter electrode is at least 10 times that of the working electrode. According to the recommendations of *ASTM* standard *G148*, an electrode potential of +541 mV against the standard hydrogen electrode (SHE) was potentiostatically adjusted in a 0.1 mol L^{-1} sodium hydroxide (NaOH) solution.[11] During the experiment, the temperature was kept constant by a temperature-controlled and electrically screened housing surrounding the permeation cell. The test solution and 0.1 mol L^{-1} NaOH were preheated at 50°C ± 1K for at least 24 h to reduce DO. Before being poured into the cell, the electrolytes were tempered to 25°C ± 1K. When the current density in the oxidation cell fell i_{BG} = 0.1 µA cm^{-2} (background current density), the charging cell was filled with oxygen-depleted solution (A or B). According to the literature, permeation measurements on steel membranes of different thicknesses determined the effective hydrogen diffusion coefficient of the steel membrane D_H.[12]

3 | RESULTS

3.1 | Search for advantageous surface conditions

Figure 1 shows metallographic longitudinal sections of the surface of CDS-1670 in delivery condition and with the modified surface conditions. Surfaces of cold-drawn prestressed wires in delivery conditions have a drawing layer covering the surface inhomogeneously. Metallographic images indicate coverage of the dark and grayish drawing layer; however, the delivery condition has layer

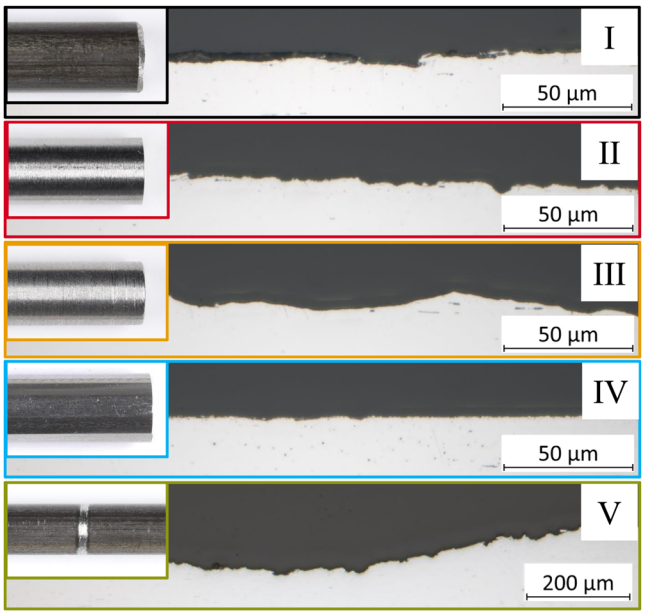

FIGURE 1 Metallographic longitudinal sections of the surface of CDS−1670 prestressing steel wires d = 7 mm in delivery condition with drawing layer (I), SiC (P80) ground (II), turned off (III), polished (IV), and drawing layer partially scratched (V). [Color figure can be viewed at wileyonlinelibrary.com]

artifacts (scratches) along the surface, originating in the cold-drawing process and transportation.

Varying surface conditions, most drawing layers can be removed. Where applicable, the surface roughness of the observed surface conditions was measured, see Table 2, and different results on roughness can be achieved:

- The surface roughness of the SiC (P80) ground condition shows significantly higher roughness values for both center roughness R_a and roughness depth R_z in the longitudinal direction compared to the as-delivered condition (factor 1.8 for R_a and factor 1.6 for R_z).
- Compared to the delivery condition, the turned surface condition shows the highest roughness in this study, with a factor of 8.5 in R_a and a factor of 4.4 in R_z.
- The polished surface condition shows a significant reduction in roughness, about 60% in R_a and 46% in R_z, compared to the delivery condition. The polishing removes most of the drawing layer, creating more homogeneous steel surfaces without significant artifacts (scratches in the drawing layer).

Despite a new surface condition being created by polishing, it does not change the prestressing steel's load-bearing cross-section and form. More homogeneous surfaces without significant artifacts and low roughness values can help homogenize the distribution of anodically and cathodically active surface areas, reducing scatter in stress corrosion tests.

The surface condition with targeted damage to the delivery surface condition could not be evaluated due to the lack of longitudinal periodicity of the surface profile. Ground and turned surfaces generally reduce the cross-section of the prestressing steel, which is highly detrimental to product testing for hydrogen stress corrosion cracking susceptibility. For this reason, comparing the delivery and polished surfaces in an electrochemical study could be particularly interesting.

The free corrosion potential E_{corr} after 30 min of free corrosion in solution B at 50°C ± 1K of the different surface conditions are shown in Figure 2. The results are the following:

- Surfaces in the delivery condition in solution B at 50°C ± 1K have a mean E_{corr} of −595 $mV_{Ag/AgCl}$.
- Samples with ground and turned surfaces have a more negative E_{corr} than samples with delivery surfaces, indicating an increase in the anodic surface fractions.
- The E_{corr} of samples with scratches is not lower than those in delivery condition.
- Samples with polished surfaces do not show a significant decrease in the E_{corr} compared to samples in the delivery condition.

E_{corr} is insufficient to evaluate corrosion activity as a function of surface conditions. For this reason, the polarization resistance R_P was determined for the different surface conditions at the same parameters, see Figure 3. The IR-drop corrected results were the following:

- The R_P for all surface conditions indicates active corroding systems. However, there are significant differences in the scattering.

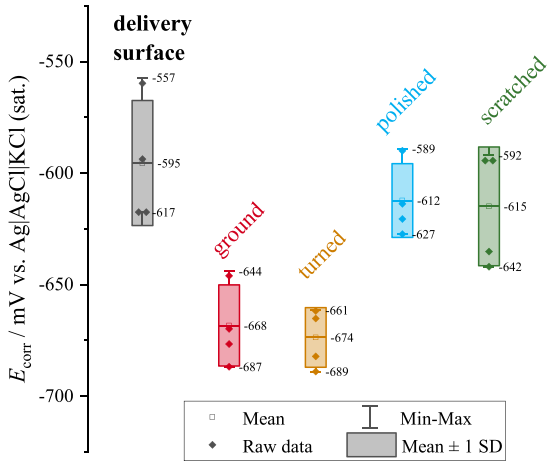

FIGURE 2 Free corrosion potential E_{corr} of CDS-1670 with varying surface conditions after 30 min of free corrosion in test solution B at 50°C ± 1K. [Color figure can be viewed at wileyonlinelibrary.com]

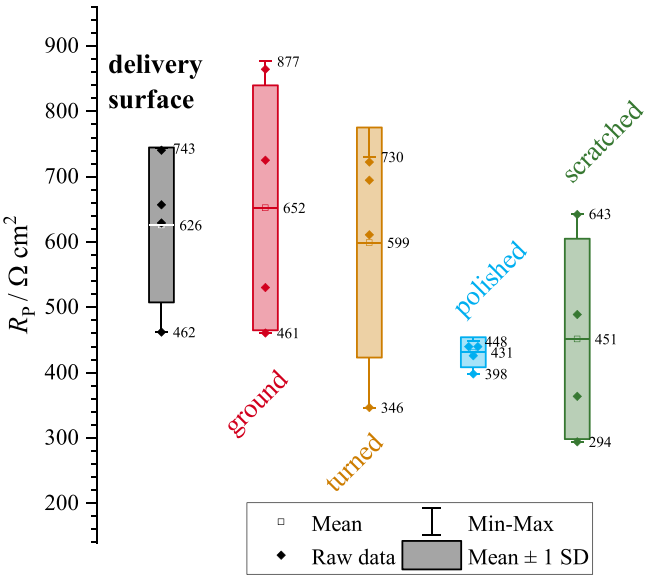

FIGURE 3 Polarization resistance R_P of varying surface conditions after 30 min of free corrosion in test solution B at 50°C ± 1K. IR-drop corrected. [Color figure can be viewed at wileyonlinelibrary.com]

- The R_P values of the ground and turned surfaces show no significant difference but a higher scatter than the delivery condition. The higher scatter could be due to an increase in the effective surface area due to the higher roughness or the presence of a modified steel surface.
- The R_P of the scratched condition is insignificantly lower than the delivery condition but with higher scattering. The scratched area acts as an anode, while the surrounding area with the delivery surface acts as a cathode. Such element formation at scratches or artifacts is problematic because it can lead to more localized corrosion and, hence, more undefined hydrogen charging.
- The polished condition shows the lowest scattering of R_P and significantly lower R_P values in this survey.
- The delivery condition has layer artifacts, where the drawing layer is missing in a local area; in this local area, the steel can directly contact the solution without the additional polarization resistance of the drawing layer.

As a result of the variation in the surface conditions, the following sections will continue with the delivery surface and the polished surface.

3.2 | Variation of electrolyte-related parameters

In the search for time-constant electrochemical corrosion characteristics that may result in constant hydrogen charging conditions, the following test parameters are varied in this section:

- Test solution A, polished
- Test solution A, delivery surface
- Test solution B, polished
- Test solution B, delivery surface

All experiments were adjusted at temperatures of the solution of either 22°C or 50°C. The free corrosion potential E_{corr} at 50°C over a test-relevant period of 70 h of free corrosion is shown in Figure 4. Figure 4 shows the mean of E_{corr} with the corresponding standard deviation (SD) as a scatter of $n = 4$ measurements. The following results can be seen:

- At 50°C, after 0.5 h, the E_{corr} of the samples with the delivery surface in solution A is, on average, $-690\ mV_{Ag/AgCl}$. Throughout 70 h of free corrosion, it is almost constant. At the time of 70 h, it is $-700\ mV_{Ag/AgCl}$.
- The E_{corr} of the samples with the polished surface in solution A is also constant on average between $-710\ mV_{Ag/AgCl}$ and $-700\ mV_{Ag/AgCl}$.
- The E_{corr} of the samples with the delivery surface in solution B drops about 50 mV from $-600\ mV_{Ag/AgCl}$ to $-650\ mV_{Ag/AgCl}$ over the period investigated.
- The E_{corr} of samples with a polished surface in solution B drops only about 25 mV from $-650\ mV_{Ag/AgCl}$ to $-675\ mV_{Ag/AgCl}$.
- Lower free corrosion potentials were measured in solution A than in solution B for both the delivered and polished surfaces.
- Compared to solution A, more extensive scattering in the range of E_{corr} was calculated with surfaces in solution B.

Basically, the pH value of solution A at 50°C is (5.1 ± 0.3), and that of solution B is (7.2 ± 0.4), see Table 3, indicating a higher corrosion activity in solution A than in solution B. More detailed information about the corrosion activity of the surfaces in the test solutions is provided by the time course of the polarization resistance R_P, see Figure 5. Here, the results are the following:

- At 50°C, the R_P values are lower in solution A than in solution B.
- The scatter of R_P is smaller in solution A than in solution B.
- In solution A, the R_P of samples with the delivery surface is lower than with the polished surface.
- In solution B, no significant difference can be seen between the surface conditions in the period up to 10 h; in the period from 10 to 70 h, the R_P (delivery surface) < R_P (polished).

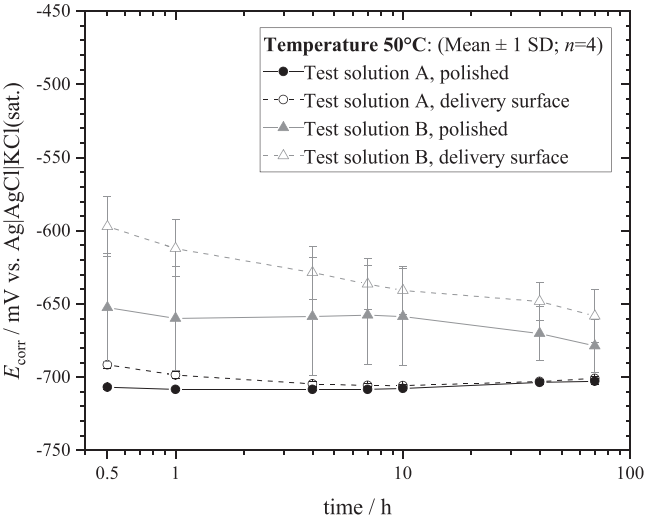

FIGURE 4 Free corrosion potentials E_{corr} at 50°C over a test-relevant period.

TABLE 3 The chemical composition and pH of test solutions A and B at 50°C ± 1K.

	Test solution A	Test solution B
Chem. composition	20 mass% NH_4SCN	Aqueous solution of K_2SO_4, KSCN, KCl (5.0 g/L SO_4^{2-}; 1.0 g/L SCN^-; 0.5 g/L Cl^-)
pH-value	(5.1 ± 0.3)	(7.2 ± 0.4)

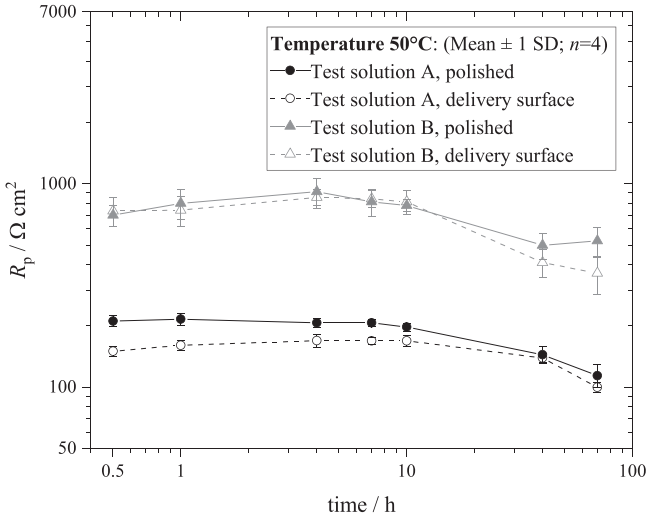

FIGURE 5 Polarization resistances R_P (IR-compensated) at 50°C over a test-relevant period.

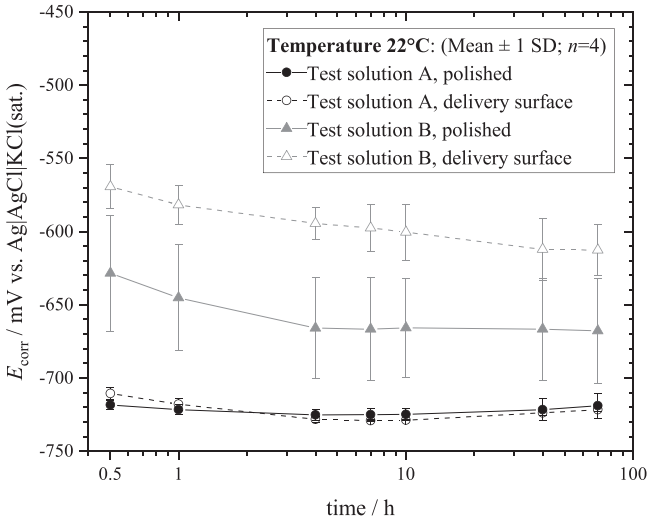

FIGURE 6 Free corrosion potentials E_{corr} at 22°C over a test-relevant period.

- All variants' R_P values are almost constant from 0.5 to 10 h. From 10 to 70 h, the R_P in both solutions decreases. In solution A, from about 200 Ω cm² to about 120 Ω cm² on samples with polished surfaces and from about 150 Ω cm² to about 100 Ω cm² on samples with delivery surfaces. In solution B, from an average of about 800 Ω cm² to about 500 Ω cm² on the polished surface condition, down to about 400 Ω cm² on delivery surface samples.

The results for the corresponding time course of E_{corr} and R_P at a reduced temperature of 22°C, are shown in Figures 6 and 7, respectively. At 22°C, the following differences from the experiments at 50°C can be seen:

- At 22°C, E_{corr} and R_P in solution A is lower than at 50°C.
- At 22°C, E_{corr} and R_P of delivery condition samples in solution B are higher than at 50°C.
- At 22°C, E_{corr} of samples with the polished surface in solution B are not significantly different from the results at 50°C.
- At 22°C, R_P of samples with polished surfaces in solution B is significantly increased compared to 50°C and increases over time.

A preheating of both solutions at 50°C was performed for 24 h to establish a constantly low equilibrium content of DO. Before the experiments, the desired experimental temperature (22°C or 50°C) was adjusted in an additional 30 min period. At the start of the experiments, DO values of approximately 3 ppm were measured in each solution.

3.3 | Charge density during free corrosion

Changes in R_P indicate changes in free corrosion current density i_{corr} assumed a constant B-value. In a Stern–Geary approach, the i_{corr} is a function of the B-value, and the R_P, see Equation (1).[13,14]

$$i_{corr} = \frac{B}{R_P}\,[\mathrm{mA\,cm^{-2}}]. \quad (1)$$

The anodic and cathodic Tafel slopes β_a, β_c [V dec^{-1}] of a current density/potential curve (polarization curve) [plotted in terms of logarithm of the current density versus potential] were determined for each experiment. The *B*-value is a combined variable of both Tafel slopes β_a, β_c and was calculated according to Stern–Geary Equation (2).

$$B = \frac{1}{2.3} \frac{\beta_a \beta_c}{(\beta_a + \beta_c)} [\mathrm{V}] \quad (2)$$

The charge density q can be obtained from the integration i_{corr} over the time of free corrosion according to Equation (3).

$$q = \int_{t=0.5\,\mathrm{h}}^{t=70\,\mathrm{h}} i_{corr}\, dt\, [\mathrm{C\ cm^{-2}}] \quad (3)$$

In Table 4, the results of q are listed. The charge density on CDS−1670 over the observed test period from 0.5 to 70 h is higher at 50°C than at 22°C and higher in solution A compared to solution B. However, a significant dependence of q on the surface condition cannot be seen.

The course of i_{corr} and *B*-value at 50°C and 22°C are shown in Figures 8–11, respectively, and the results were the following:

- Figures 8 and 10 show higher i_{corr} values in solution A than in solution B.

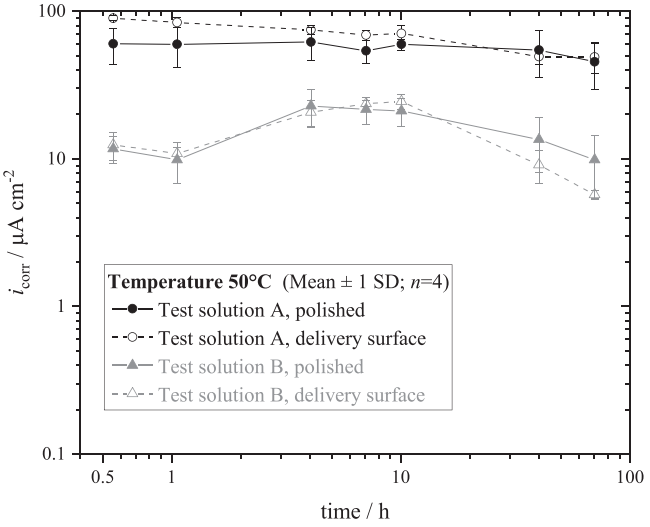

FIGURE 8 Free corrosion current density i_{corr} results at 50°C.

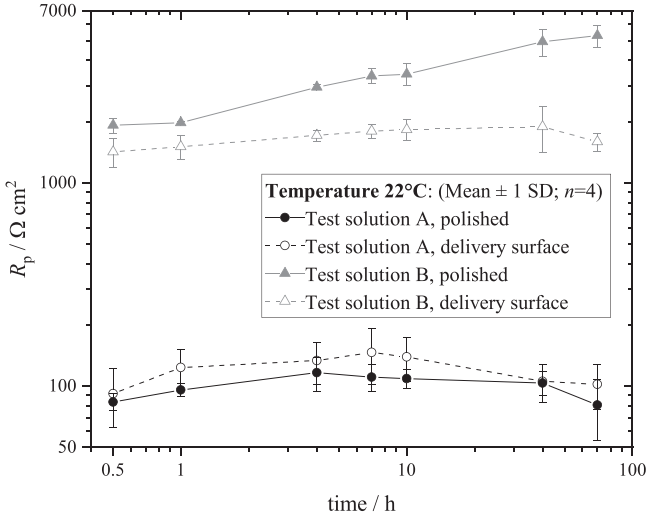

FIGURE 7 Polarization resistances R_P (IR-compensated) at 22°C over a test-relevant period.

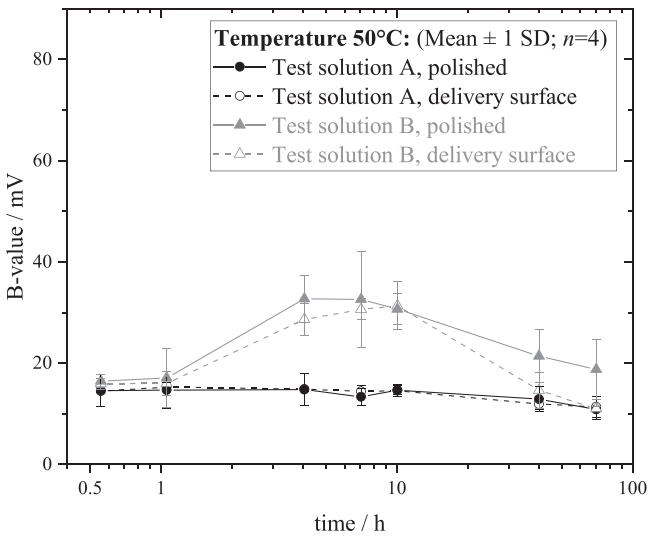

FIGURE 9 *B*-values at 50°C.

TABLE 4 Charge density q on CDS-1670 during free corrosion over a test-relevant period from 0.5 h until 70 h.

	Temperature 22°C	Temperature 50°C
Test solution A, polished	5.49 C cm^{-2}	13.58 C cm^{-2}
Test solution A, delivery condition	4.76 C cm^{-2}	14.31 C cm^{-2}
Test solution B, polished	0.97 C cm^{-2}	3.80 C cm^{-2}
Test solution B, delivery condition	1.35 C cm^{-2}	3.30 C cm^{-2}

- In Figures 8 (at 50°C) and 10 (at 22°C), i_{corr} has an approximate linear course in solution A.
- On the other hand, solution B displays a nonlinear course of i_{corr}.
- At a temperature of 50°C (Figure 8), samples with polished surfaces and delivery surfaces in solution B show a maximum in i_{corr}, around 5–10 h of free corrosion. This maximum can lead back to the course of the *B*-value (see Figure 9).
- In contrast to the course of i_{corr} and *B*-value at 50°C in solution B, a linear course of i_{corr} and *B*-value can be seen at 22°C (Figures 10 and 11) for samples with the delivery surface in solution B. In Figure 10, the i_{corr} of samples with polished surfaces in solution B at 22°C decreases after 10 h of free corrosion due to the rise of R_P (Figure 7). The delivery surface layers in solution B may seem more stable at a temperature of 22°C than at 50°C, which leads to lower i_{corr} (compare Figure 10 [at 22°C] with Figure 8 [at 50°C]) and also lower q values (see Table 4).

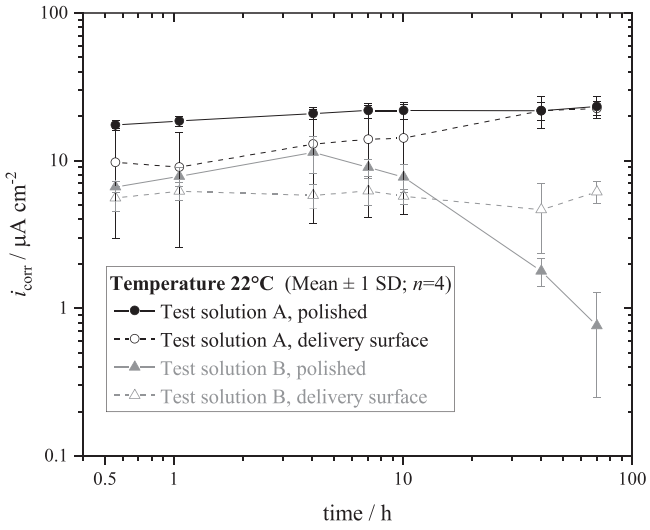

FIGURE 10 Free corrosion current density i_{corr} results at 22°C.

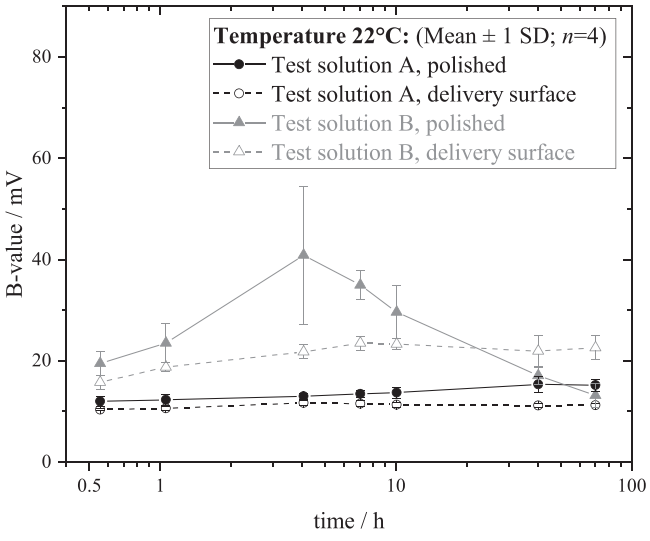

FIGURE 11 *B*-values at 22°C.

However, the results show that the most uniform testing conditions can be achieved in solution A at a temperature of 22°C on samples with polished surfaces since the course of i_{corr} (see Figure 10) is the most evenly linear form on a constant level. The scattering is low compared to experiments at a temperature of 50°C.

3.4 | Influence of test solutions on hydrogen charging

In permeation measurements with type 1.0978 unalloyed steel membranes, after filling the charging cell, hydrogen adsorption occurs on the steel membrane due to corrosion. Adsorbed hydrogen can be taken up (absorbed) into the material in the next step. With a time delay, the total current increases due to the oxidation of the permeable hydrogen on the oxidation side. The permeation current I_P is the difference between the total current I_{total} and the background current I_{BG}. As an example, Figure 12 shows both the course of the permeation current I_P on the oxidation side as well as the free corrosion potential E_{corr} in the charging cell for a free corrosion hydrogen charge in solution A at 25°C ± 1K. Figure 12 shows that the

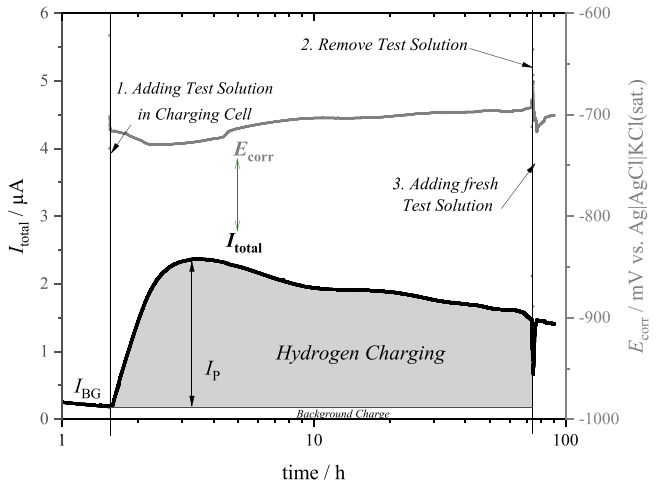

FIGURE 12 Time course of the total current I_{total} on the oxidation side of an unalloyed steel membrane d = 0.05 mm during free corrosion in test solution A at 25°C ± 1K (black curve) and the corresponding free corrosion potential E_{corr} over time in the charging cell (gray curve).

permeation current—and thus, integrated over time, the hydrogen charge—moves inversely to the time course of the corrosion potential with a delay.

The numerical results of the permeation measurements are shown in Table 5. The permeation measurements were performed at 25°C ± 1K for better comparability with the literature hydrogen equilibrium concentration. After injecting the test solution into the charging cell, there is a time delay in the passage of the hydrogen through the steel membrane, resulting in an increase in I_P measured on the oxidation side. The time to hydrogen leakage and maximum permeation current is reached earlier in solution A than in solution B, see Table 5. This indicates a delay in hydrogen adsorption in solution B compared to solution A. Since I_P is a direct measure of the hydrogen flux through the steel membrane, Equation (4) can calculate a (subsurface) hydrogen concentration $c_{H,e}$ in the charging cell of the steel membrane.

$$c_{H,e} = \frac{I_{P,ss} d}{F D_H A_{geo}} [\text{mol(H)cm}^{-3}\text{(Fe)}]. \quad (4)$$

The $I_{P,ss}$ is the steady-state permeation current, F is the Faraday constant, and D_H is the material-specific effective hydrogen diffusion coefficient. The hydrogen diffusion coefficient of the unalloyed steel membrane with material number 1.0978 was determined to be $D_H = (6.0 \pm 0.5) \cdot 10^{-7}$ cm^2 s^{-1}. Using $I_{P,ss}$, the hydrogen activities of the test solutions were calculated using Equation (4) in Equation (5), and the results are listed in Table 5.

$$a_H = \frac{c_{H,e}}{c_{H,0}} \quad (5)$$

The equilibrium interstitial hydrogen concentration in the trap-free iron at a partial pressure of $P_{H_2,0} = 1$ bar at 25°C is assumed to be $c_{H,0} = 8.425 \cdot 10^{-9}$ mol (H) cm^{-3} (Fe).[15]

4 | SUMMARY AND DISCUSSION

Regarding the pH value as a major impact on potential formation, the potential of prestressing steels in solution A should be higher than in solution B. Based on the Nernst equation, the tendency of the potential position can be estimated as a function of the pH value, see Equation (6), where pH = −log[H$^+$], E_0 = standard electrode potential, T= temperature, R = gas constant, z = charge number, and F = Faraday constant.

$$E = E_0 - \frac{2,3RT}{zF} \text{pH [V vs. SHE]}. \quad (6)$$

The linear dependence of the potential versus the SHE over pH calculated from Equation (6) for hydrogen evolution (HE) at temperatures 22°C and 50°C is shown in Figure 13. The drawings of the temperature- and pH-dependent free corrosion potential levels for solutions A and B show that the HE tends to be the cathodic partial reaction in solution A. In contrast, the surfaces in solution B have a less clear tendency toward HE. Due to the low DO content of 3 ppm, the oxygen reduction (OR) must be inhibited. Thus, the thermodynamic approach is not applicable, see Figure 13. However, it indicates that either the anodic or cathodic partial reaction is inhibited. The anodic partial reaction occurs according to Equation (7).

$$\text{Fe} \rightarrow \text{Fe}^{2+} + 2\text{e}^-. \quad (7)$$

The cathodic partial reaction for forming adsorbed hydrogen $H_{ad.}$ takes place according to Equation (8).

$$\text{H}^+ + \text{e}^- \rightarrow \text{H}_{ad.}. \quad (8)$$

Next, adsorbed hydrogen $H_{ad.}$ can absorb into the prestressing steel microstructure (hydrogen charging). In a further step, adsorbed hydrogen can recombine, forming

TABLE 5 Results of permeation measurements with a membrane made of unalloyed steel d= 0.05 mm with free corrosion in test solutions A and B at 25°C ± 1K.

	$t(i_{P,max})$ [h]	$I_{P,ss}$ [μA]	a_H
Test solution A	(0.64 ± 0.25)	(0.98 ± 0.17)	(8.90 ± 1.54)
Test solution B	(17.87 ± 3.17)	(0.09 ± 0.03)	(1.08 ± 0.44)

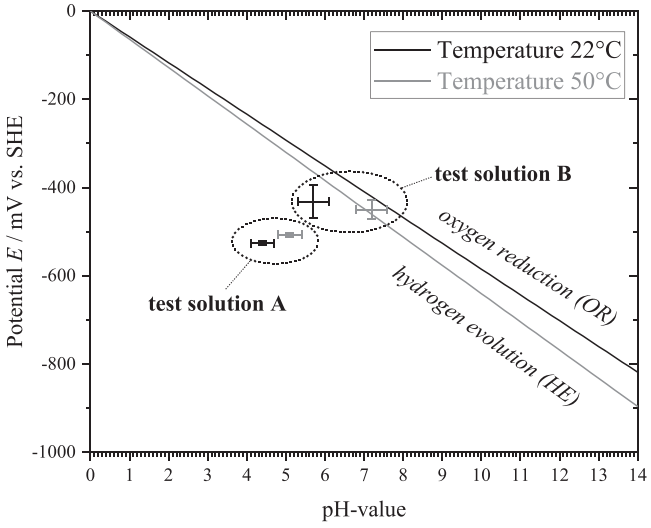

FIGURE 13 Temperature-dependent potential versus pH plot for hydrogen evolution (HE) and oxygen reduction (OR).

molecular hydrogen, which is described elsewhere.[16] The thiocyanate (SCN^-) in solutions A and B inhibit the recombination, though SCN^- is more concentrated in solution A than in solution B. However, the cathodic partial reaction in both solutions proceeds predominantly according to Equation (8). The formation of a surface layer in solution B could affect the reversed potential levels between A and B due to more positive charge carriers at the surface layer/solution phase boundary. A positively charged surface layer inhibits the charge separation, according to Equation (7). In the case of surface layer formation, potential levels can be reached that cannot be described with thermodynamic equations, such as the Nernst equation. The potential here depends on the kinetics of the interfacial reactions – potential drop across the compact and diffuse Helmholtz layer.

The more extensive scattering range of the E_{corr} and R_P in solution B compared to solution A indicates the formation of a non-homogenous surface layer. It can be seen that the samples in solution A are significantly more active in terms of corrosion (lower R_P) than those in solution B, see Figures 5 and 7.

Based on the knowledge that HE takes place as cathodic partial reaction, a higher charge density q during free corrosion in solution A (the integral of i_{corr}) can lead to a higher hydrogen charging intensity than in solution B. This was approved by hydrogen permeation measurements, in which the steady-state hydrogen activity at 25°C ± 1K of solution A is significantly higher than that of solution B. The steady-state hydrogen activity in solution B at 25°C ± 1K is calculated to be 1.08 ± 0.44. In a similar observation of solution B, steady-state hydrogen activities of 1.13 to 2.12 were calculated for a test temperature of 50°C.[17]

The charge density q in the observed time range experiments is mostly a factor 2.5–4.0 higher at a temperature of 50°C compared to 22°C, see Table 4. The calculated i_{corr} values in solution A show less scattering at 22°C than those at 50°C and more constant values over time (compare solution A lines of Figure 8 and Figure 10). Consistent i_{corr} values for polished surfaces in solution A at 22°C, calculated by Equation (1), are the most critical for time to fracture scattering.

This is a hint that polishing the surfaces reduces the scattering of R_P, and a temperature control at 50°C is unnecessary in solution A. The temperature reduction will not shorten the time to fractures; however, it helps set more constant testing conditions.

Basically, the polishing step reduces the roughness and vanishes micro crevices. This may homogenize the distribution of anode and cathode areas. A predicted model of corrosion surface characteristics in both test solutions can be concluded, and a visualization of the delivery and polished surface is shown in Figure 14.

In the case of solution B, neither polishing nor a temperature of 22°C can help reduce the scattering or consistency of corrosion quantities. Significant changes in E_{corr}, R_P, i_{corr}, and B-values were determined, probably due to surface layer formation and non-homogenous distribution of anodic and cathodic areas. Table 5 shows

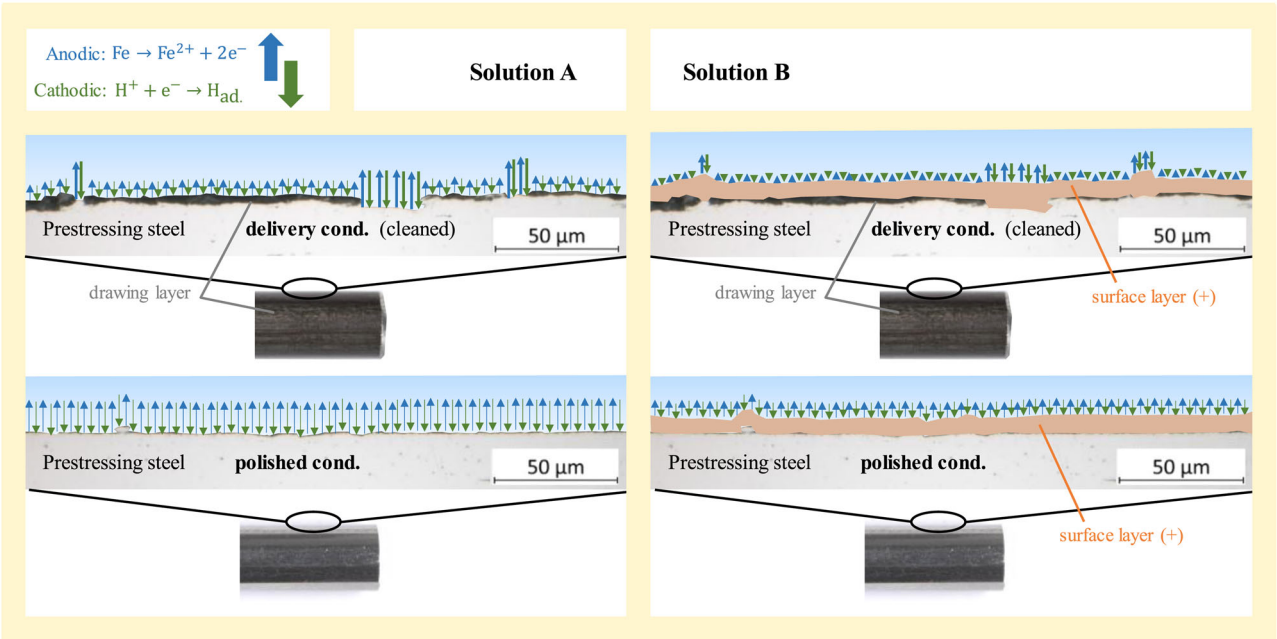

FIGURE 14 Model of corrosion surface characteristics predicted from this paper's findings at a constant solution temperature. [Color figure can be viewed at wileyonlinelibrary.com]

that the maximum hydrogen permeation in solution B takes about 17 h through a thin 0.05 mm membrane. In comparison, solution A induces the maximal hydrogen permeation in 0.6 h. In solution B, hydrogen is charged later to the prestressing steel. At the same time, there are less intense corrosion current densities and a minor hydrogen charging intensity (hydrogen activity a_H) compared to solution A.

Basically, a pre-heating of test solutions for 24 h at 50°C in an extra glass vessel is necessary to ensure the low DO content before the experiments, to reproduce the findings of this paper.

5 | CONCLUSIONS

This paper's findings show the influencing parameters for stress corrosion test methods according to ISO 15630-3 by describing the corrosion systems. The scatter seems to be dominated by surface conditions. Both the effect of microstructure and surface conditions are relevant to understanding the failure mechanism. The fact that both aspects can now be studied allows manufacturers to understand how to develop more robust steel.

As expected, test solution A is more suitable for factory production control and continuous surveillance tests by third parties. Also, solution A should be used for initial approval tests due to the corrosion characteristics mentioned above. The recommended modifications of the free corrosion test in solution A can lead to potentially slightly longer testing times, but may reduce the more important scattering of results. The use of solution B in quality production control and continuous surveillance cannot be recommended because modifying surface conditions and temperature adjustments do not generate the desired low scattering of results.

A test setup using pre-heated solution A (for 24 h at 50°C in an extra glass vessel) testing polished samples at a reduced temperature of 22°C is a reasonable modification for more uniform test conditions, which should be observed in future stress corrosion tests.

6 | OUTLOOK

The permeation measurements show the difficulty of the test method in the presence of free corrosion. Even when solution A is used, the maximum possible hydrogen activity is only reached after about 0.6 h, maybe due to the time-dependent formation of the anodic and cathodic areas (Table 5). This is still disadvantageous for a test method in which the time to fracture is the test quantity. It would be better to control hydrogen charging during the tests entirely. Therefore, the possibility of using cathodic polarization could be addressed in future studies to improve the stress corrosion test for prestressing steels, setting conditions for hydrogen charging right back from the test's start.

AUTHOR CONTRIBUTIONS

Lando Seifert was involved in the conceptualization, investigation, and writing of—the original draft. Andreas Grunewald was involved in the investigation. Thoralf Müller and Gino Ebell were involved in project management, review, and editing.

ACKNOWLEDGMENTS

The authors thank the German Federal Ministry for Economic Affairs and Climate Action (BMWK) for funding through the WIPANO initiative, Knowledge and Technology Transfer via Patents and Standards, FKZ: 03TNH019/A.

CONFLICT OF INTEREST STATEMENT

The authors declare no conflict of interest.

DATA AVAILABILITY STATEMENT

The data that support the findings of this study are available from the corresponding author upon reasonable request.

ORCID

Lando Seifert http://orcid.org/0009-0006-3486-9793
Gino Ebell http://orcid.org/0000-0002-6006-2460

REFERENCES

[1] Fédération Internationale du Béton (FIB), Task Group 9.5, U. Nürnberger, Technical Report on Influence of Material and Processing on Stress Corrosion Cracking of Prestressing Steel—Case Studies, **2003**.
[2] J. Lingemann, *Ph.D. Thesis*, TU München, Germany, **2010**.
[3] ISO 15630-3:2019: Steel for the Reinforcement and Prestressing of Concrete—Test Methods—Part 3: Prestressing Steel.
[4] prEN 10138-1, -2, -3, -4:2000: Spannstähle, Teil 1: Allgemeine Anforderungen, Teil 2: Draht, Teil 3: Litze, Teil 4: Stäbe.
[5] J. Mietz, K. Pasewald, B. Isecke, Untersuchungen zum wasserstoffinduzierten Sprödbruch vergüteter Spannstähle, Schlussbericht zum DIBt-Forschungsvorhaben IV 1-5-651/92, Berlin **1998**.
[6] J. Mietz, *Materials and Corrosion* **2000**, *51*, 80.
[7] J. Mietz, J. Fischer, *Ringversuch zur Prüfung der Spannungsrisskorrosion an Spannstählen*, Bauforschungsbericht T 3306, Fraunhofer IRB Verlag, Stuttgart **2014**.
[8] B. Isecke, *Test Methods for Assessing the Susceptibility of Prestressing Steels to Hydrogen Induced SCC* **2004**, EFC Publications Number 37, Maney, London.
[9] DIN 1045-3:2023: Concrete, Reinforced, and Prestressed Concrete Structures—Part 3: Execution of Structures.
[10] J. Mietz, B. Isecke, *Mater. Corros.* **2002**, *53*, 373.

[11] ASTM International, *Standard Practice for Evaluation of Hydrogen Uptake, Permeation, and Transport in Metals by an Electrochemical Technique*, Designation G148-97, Beuth Verlag, Berlin **2011**.
[12] M. A. V. Devanathan, J. Stachursky, *Proc. Roy. Soc. Lond. A* **1962**, *270*, 90.
[13] M. Stern, A. L. Geaby, *J. Electrochem. Soc.* **1957**, *104*, 56.
[14] M. G. Fontana, *Corrosion Engineering*, 3rd ed., McGraw-Hill Book Co, Singapore **1987**.
[15] J. Moersch, *Mater. Corros.* **2003**, *54*, 419.
[16] M. Truschner, A. Trautmann, G. Mori, *BHM Berg- und Hüttenmännische Monatshefte* **2021**, *166*, 443.
[17] J. Moersch, *Zur wasserstoffinduzierten Spannungsrisskorrosion von hochfesten Spannstählen*, DAfStb, Beuth, Berlin, **2005**.

How to cite this article: L. Seifert, A. Grunewald, T. Müller, G. Ebell, *Mater. Corros.* **2024**, 1–13. https://doi.org/10.1002/maco.202313948